Schweizerische Eidgenossenschaft
Confédération suisse
Confederazione Svizzera
Confederaziun svizra

Eidgenössisches Departement für
Umwelt, Verkehr, Energie und Kommunikation UVEK

Bundesamt für Energie BFE

SOLAR-TEP

MATERIALENTWICKLUNG FÜR SOLAR-THERMOELEKTRISCHE STROMERZEUGER

Schlussbericht 2008

Ausgearbeitet durch

Rosa Robert and Anke Weidenkaff
Solid State Chemistry and Catalysis, Empa-Swiss Federal Laboratories for Materials Testing and Research
Ueberlandstrasse 129, CH-8600, rosa.robert@empa.ch, anke.weidenkaff@empa.ch, www.empa.ch

Impressum

Datum: *6. Juni 2008*

Im Auftrag des Bundesamt für Energie
Forschungsprogramm Elektrizitätstechnologien und -anwendungen

Mühlestrasse 4, CH-3063 Ittigen

Postadresse: CH-3003 Bern

Tel. +41 31 322 56 11, Fax +41 31 323 25 00

www.bfe.admin.ch

BFE-Bereichsleiter, thilo.krause@bfe.admin.ch

BFE-Vertrags- und Projektnummer: *101706/152070*

Bezugsort der Publikation: www.energieforschung.ch / www.electricity-research.ch

Inhaltsverzeichnis

Zusammenfassung

In dieser Arbeit werden verschiedene Kobaltate hinsichtlich potentieller thermoelektrischer Anwendungen bei hohen Temperatur untersucht. Die komplexen Kobalt-Oxidphasen werden mittels „Chimie douce“ und klassischer Methoden synthetisiert. Die resultierenden potenziellen thermoelektrischen Materialien werden bezüglich ihrer Kristallstruktur, Mikrostruktur, Zusammensetzung und Thermostabilität mittels verschiedenen Methoden wie EXAFS, XRPD, EM/ED, TGA, XRF, HGE und DSC charakterisiert.

Der Seebeck Koeffizient, die thermische Leitfähigkeit und der elektrische spezifische Widerstand von polykristallinen Kobaltaten mit Perowskit- ähnlicher oder geschichteter Struktur werden in einem weiten Temperaturbereich evaluiert. Die elektrischen Transporteigenschaften epitaktischer $La(Co,Ni)O_3$ PLD-Filme wurden mit den Resultaten der polykristalline Pellets verglichen und ergaben eine geringfügig bessere thermoelektrische Leistung bei hohen Temperaturen.

Die große Flexibilität der Perowskitstruktur ermöglicht eine Änderung der chemischen Zusammensetzung und erlaubt somit eine Feinabstimmung der physikalischen Eigenschaften. In dieser Studie wird der Einfluss von *A*- und *B*-Position Substitutionen im $LaCoO_3$ System untersucht. Die Substitutionen auf der *B*-Position haben einen maßgeblichen Einfluss auf die Ladungsträgerkonzentration und spielen eine wichtige Rolle bei der Erhöhung der elektrischen Leitfähigkeit. Außerdem können *p*- und *n*-leitende Phasen durch aliovalente Oxidationszustände erzeugt werden. Ti- substituierte Kobaltate zeigen reduzierte Wärmeleitfähigkeiten, welches einer Zunahme der Gitter-Unordnung in diesen Phasen zugeschrieben werden kann. Weiterhin wird gezeigt, dass durch Ersatz der Lanthanid-*A*-Kationen in $LnCoO_3$ mit kleineren Selten-Erdelementen die Thermokraft erhöht werden kann. Dieses resultiert aus der Stabilisierung der Co^{3+} Ionen im low-spin Zustand.

Die sehr hohen Seebeck- Koeffizienten perowskitartiger Phasen, wie auch die der geschichteten Kobaltite, können durch Verwendung der Heikes Formel quantitativ beschrieben werden. Daraus lässt sich schließen, dass die Thermokraft in Kobaltaten maßgeblich von der Entartung der Spin-Zustände, bzw. der elektronischen Struktur der Co-Ionen abhängt. Die Ergebnisse zeigen das Potenzial von $La(Co,Ti)O_3$ und $Dy(Co,Ni)O_3$ Phasen für mögliche Anwendungen als Hochtemperatur-Thermoelektrika.

Abstract

Cobaltate phases are suitable materials for thermoelectric applications at high temperature. Complex cobalt oxide phases are synthesized by “Chimie douce” and classical methods. These potential thermoelectric materials are characterized with respect to their crystal structure, microstructure, composition, and thermal stability by EXAFS, XRPD, EM/ED, TGA, XRF, HGE and DSC.

The Seebeck coefficient, thermal conductivity and electrical resistivity of polycrystalline cobaltates with perovskite-type and layered-cobaltite structure are evaluated in a wide temperature range. The electrical transport of epitaxial $La(Co,Ni)O_3$ thin films grown by pulsed laser deposition are compared with its bulk counterpart.

The perovskite structure possesses a very high degree of compositional flexibility being able to tolerate a wide variety of cations on both the *A*- and *B*-site and allowing the fine tuning of physical properties. In this experimental study, the influence of *B*-site substitution in the $LaCoO_3$ system is reported. In the studied *B*-site substituted $LaCoO_3$ phases, the charge carrier concentration plays an important role in the enhancement of the electrical transport. The comparison of the electrical transport of $La(Co,Ni)O_3$ thin films with the polycrystalline phase reveals that the thin films display better thermoelectric performance at high temperatures.

The large Seebeck coefficient exhibited by both perovskite-type and layered cobaltite phases is analysed using the Heikes formula. It can be concluded that the thermopower in cobaltate phases is governed by the spin and orbital degeneracy of the electronic states of the Co ions.

1. Introduction

Over the last twenty years intensive research is being done in the implementation of “green” energy sources such as solar power. Nowadays, the major energy consumption comes from limited and non-renewable resources such as fossil fuels. The use of this energy releases polluting emissions into the atmosphere which generate unpredictable influences on our environment. Additionally, they draw on finite resources. In contrast, renewable energy resources like solar energy are constantly replenished.

The Solar-TEP project is based on the idea of the potential use of concentrated solar heat [1-3] as energy source for Solar Thermoelectric Generators (Solar-TEG). Thermoelectric power generation, i.e. direct energy conversion from heat into electricity, can be realized by means of thermoelectric converters which consist on *p*- and *n*-type thermoelements connected electrically in series and thermally in parallel. As is shown in Figure 1, thermoelectric generators and refrigerators are heat engines which make use of the Seebeck effect (see Figure 1a) and the Peltier effect (see Figure 1b), respectively.

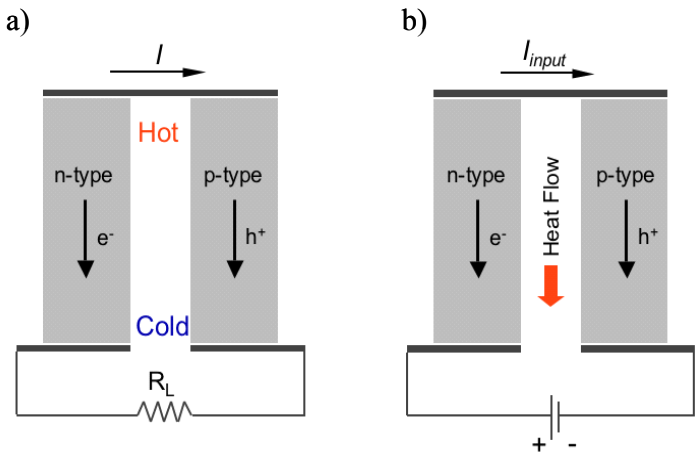

Figure1: a) Thermoelectric generator and b) thermoelectric refrigerator.

2. Objective and Goals

Good thermoelectric materials (*p*- and *n*-type thermoelements) involve a trade-off among the three factors in the thermoelectric Figure of merit $Z = S^2/\rho\kappa$, combining a high thermopower S and low electrical resistivity ρ with low thermal conductivity κ: Recent thermoelectric research is focused on searching materials with large S, low ρ, and low κ in order to realize an efficient conversion of thermal energy into electrical energy.

“Classic” thermoelectric materials such as bismuth tellurides and Si-Ge alloys display good thermoelectric properties (ZT ~ 1.2). However, their practical application to power generation in the temperature range of 600 K < T < 1000 K is limited due to problems such as low melting- decomposition-, oxidation or temperature stability, and high toxicity.

The present work is focused on the development of novel functional materials with enhanced Figures of merit, high temperature stability (T ≥ 400 K), and without harmful elements.

The discovery of a large thermopower (S_{300K} = + 100 µV/K) in the metallic oxide Na_xCoO_2 [4] followed by the recent report of superconductivity in the $Na_xCoO_2{*}H_2O$ [5] has shown the great potential of these and related oxides as thermoelectric materials. Since this time, numerous studies have been

devoted to the investigation of the thermoelectric properties of different related families of oxides. High thermal and chemical stable materials in air can be found among ceramic oxides, which open new lines of investigation directed to the finding of materials for high temperature thermoelectric applications.

The state-of-the-art of thermoelectric oxide converters display low conversion efficiency. But, if the thermoelectric recovery of waste heat and the use of “free” energy (Solar) are considered, which does not involve the cost of thermal input, the low conversion efficiency is not a serious disadvantage. Additionally, thermoelectric oxide devices are a very attractive alternative to the conventional devices based on materials which can not operate at high temperatures (T ~1000 K) in air because they are not stable. Moreover, most of them are highly toxic and low in abundance in natural resources. On the contrary, thermoelectric oxide devices have the potential to be realised on the basis of low cost materials with low toxicity.

3. Method

The thermoelectric materials are prepared by different synthesis methods and characterized by the use of several techniques. Their crystallographic structure is characterized by X-ray Powder Diffraction (XRPD), X-ray Absorption Spectrometry (XAS), and Electron Diffraction (ED). The study of the nanostructure, texture and microstructure is performed by Scanning- and Transmission Electron Microscopy (SEM, TEM). The metal / cationic composition is determined by in-situ EDX/TEM and by X-ray Fluorescence (XRF). The oxygen content is analyzed with the Hot Gas Extraction (HGE) and the reduction methods. The thermal stability of the compounds is evaluated by Thermogravimetric Analysis (TGA). Heat transport properties, heat capacity c_p and thermal diffusivity α are determined by Differential Scanning Calorimetry (DSC) and laser flash method (LFM), respectively. The electrical resistivity ρ and Seebeck coefficient S measurements are performed in a wide temperature range. The low temperature studies are done using the Physical Property Measurement System (PPMS), and the high temperature measurements are done using the RZ2001i unit (Ozawa science).

Thermoelectric ***polycrystalline materials*** e.g. $LaCo_{1-x}Ni_xO_3$ ($0.0 \leq x \leq 0.30$), $LaCo_{1-x}Ti_xO_3$ ($0.01 \leq x \leq 0.50$), $LnCo_{0.95}Ni_{0.05}O_3$ (with Ln = La, Pr, Nd, Sm, Gd and Dy), $Ca_3Co_4O_9$ and substituted $Ca_3Co_4O_9$ are prepared by soft chemistry (“Chimie douce”) routes like the citrate-complex and the polymeric complex methods. Single phase ternary and quaternary oxides are formed in a combustion process of tailor-made complex precursors containing a premix of the cations on a molecular level [6, Weidenkaff, 2004 #105]. Soft-chemistry synthesis offers molecular mixing of the reactants, which provides a reactive environment during the course of subsequent heating and decomposition. The advantages of this synthesis approach compared to the conventional solid state reaction method are a high purity, a good homogeneity through mixing the starting materials at the molecular level in solution, a lower reaction temperature (T = 873 K) because no diffusion processes are necessary, a shorter heating time, and an enhanced ability to control particle size.

The soft chemistry process involves the formation of stable metal chelate complexes with certain α-hydroxycarboxylic acids such as citric acid (CA) where the metal element is e.g. Co. The advantage of using citric acid as ligand is the formation of stable complexes with many cations [7-9].

In the citric acid complex method, stoichiometric amounts of metal nitrates, carbonates or oxides, and citric acid are dissolved in water solution to form the desired cation-CA complexes (precursors). Metal oxides are previously dissolved in concentrated nitric acid. The final polycrystalline compounds are obtained by thermal decomposition of the corresponding precursors.

Epitaxial thin films grown on inactive substrate materials offer a suitable alternative to large single crystals as "two-dimensional" crystal and the possibility to study the influence of the dimensionality on the thermoelectric properties. $LaCo_{0.92}Ni_{0.08}O_3$ thin films are grown on MgO substrates by Pulsed Laser Deposition (PLD) technique. Thin films are characterized concerning crystallinity, morphology and composition. The transport properties are compared with the parent polycrystalline phase.

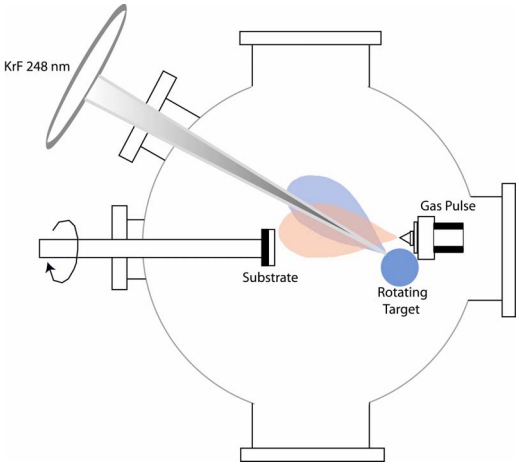

Figure 2: Scheme of the pulsed reactive crossed-beam laser ablation (PRCLA) setup. A synchronized reactive gas pulse interacts close to the target with the ablation plumes. The plasma species are deposited on a rotated heated substrate.

$LaCo_{0.92}Ni_{0.08}CoO_3$ thin films of different thickness (~ 86 nm, ~220 nm, and ~ 395 nm) were grown on MgO (100) substrates by Pulsed Reactive Crossed-beam Laser Ablation (PRCLA), (see Figure 2). PRCLA is a variation of PLD. In PRCLA, the ablation process is supplemented by a reactive gas which may affect the ablation plume species in the gas phase [10-12]. The $LaCo_{0.92}Ni_{0.08}CoO_3$ films were deposited using a KrF excimer laser (λ = 248 nm, 20 ns pulse width and variable number of pulses) with a laser fluence of 3.0 J/cm2 and a repetition rate of 10 Hz. The target material was produced from the pressed and sintered $LaCo_{0.92}Ni_{0.08}CoO_3$ powders prepared by soft chemistry method as described above.

The best method to determine an atomic arrangement with a high accuracy and precision is based on ***diffraction techniques*** using e.g. X-rays. Fine powders consist of small particles with a particle size ranging from 25 nm to 350 nm diameter. The small size of the crystallites makes the use of structural characterization methods with high spatial resolution such as ***High Resolution Electron Microscopy*** (HRTEM) and ***Electron Diffraction*** (ED) necessary. Additionally to X-ray Absorption Spectroscopy (XAS).

Valence shift and coordination environment of metal ions *by* ***X-ray Absorption Spectroscopy*** (XAS). XAS analysis makes possible to obtain information pertaining to the chemical coordination environment (local structure) of the absorbing atom independently of the particle morphology. A shift in the *K*-edge position of the metal ion can be used to qualitatively estimate the ionic state.

Thermoelectric properties measurements: The electrical resistivity ρ and the Seebeck coefficient S measurements were done during heating-and-cooling cycles with heating steps of 20 K and in the temperature range of 330 K ≤ T ≤ 1240 K, using the RZ2001i unit of Ozawa science (see Figure 3a). The measurements were performed on bar-shaped sintered pellets with dimensions of A ≈ 2*2 mm^2 and length between 5- 10 mm. Figure 3b represents in more detail the experimental set-up where two electrical contacts are placed at the ends of the sample bar and the two others on the sample body.

The Seebeck coefficient was measured by a steady-state method, in which a well defined temperature gradient (4 K < ΔT < 10 K) is applied to the sample by cooling one end with air. The temperature gradient is measured by two thermocouples (Pt/Pt+13% Rh) attached to the platinum layer contacts, which record the potential difference ΔV. The Seebeck coefficient results from the relation $S = \Delta V/\Delta T$.

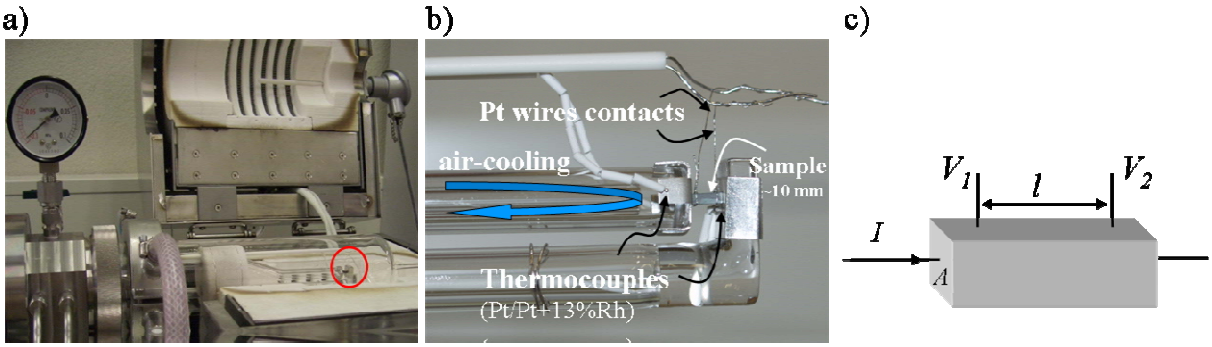

Figure 3: a) RZ2001i unit for the Seebeck coefficient and electrical conductivity measurement in the temperature range of 330 K ≤ T ≤ 1273 K, b) magnification image of the sample holder with the description of measurement parts, and c) Schematic representation of the measurement of electrical resistivity.

The electrical resistivity was measured by the DC four-probe method as displayed in Figure 3c. The two platinum contacts touching the ends of the sample supply the current I and the two platinum wires looped around the bar measure V. The resistance of the conductor R is then obtained by applying Ohm's law $I = V/R$. Knowing the dimensions of the bar and the distance l between the wire contacts, the electrical resistivity can be calculated by $\rho = RA/l$, where A is the cross sectional area of the bar.

At each temperature, the Seebeck coefficient and electrical resistivity were measured five times. The results should describe a linear fit with a correlation factor in the range 0.999 ≤ r ≤ 1.0, to ensure the quality of the measured properties. S and ρ is obtained from the slopes. In the ρ measurements, the polarity of the supplied current is reversed. The Seebeck coefficient of the sample is finally obtained after extracting the contribution of the thermocouple ($S_{sample} = S_{measured}-S_{Pt}$).

At low temperature (T ≤ 400 K), Seebeck coefficient and electrical resistivity measurements were performed using the Physical Properties Measurement System (PPMS) from Quantum Design.

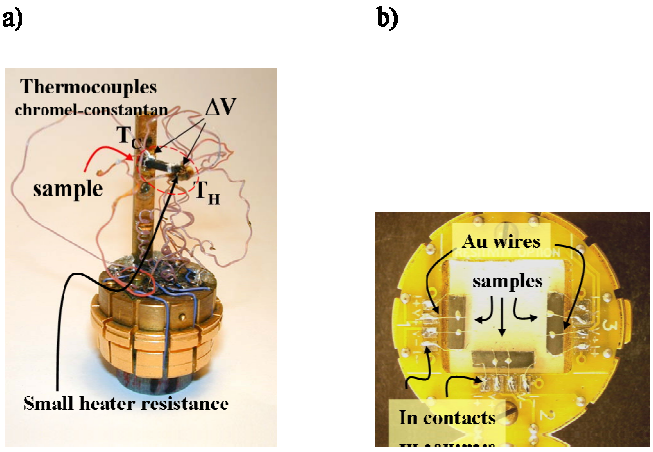

Figure 4: Physical properties measurement system (PPMS), a) Seebeck coefficient option design by Dr. J. Hejtmanek, at CRISMAT Laboratory and b) DC resistivity option.

The measurement of the Seebeck coefficient *S* was performed using a modified PPMS sample holder designed by Dr. J. Hejtmanek at the Institute Of Physics (ASCR, Prague) and at the CRISMAT Laboratory in Caen (France) in the temperature range of 2 K ≤ T ≤ 320 K. The Seebeck coefficient was measured by a steady-state method Figure 4a describes the measurement configuration. A temperature gradient ΔT is applied to the sample using a small heater resistance (R = 3.3 kΩ) attached to one of the ends. Two thermocouples of type E (chromel-constantan) are used to measure the temperature at the hot side T_H and cold side T_C. The Seebeck coefficient of the sample is obtained by the relation $S = \Delta V/\Delta T$ after subtracting the contribution of the thermocouple to the measured *S*.

The electrical resistivity *ρ* was measured by the four-probe method as shown in Figure 4b, and the *ρ* values are obtained applying the relation. The DC measurements were performed in AC mode, in which a DC current is applied to the sample and a potential drop is recorded. Then, the DC current is reversed and the potential drop is recorded again.

Figure 4b shows the DC resistivity puck. The indium contacts are deposited by ultrasounds on the sample holder and are contacted to the sample through Au wires attached with Silver paste. The electrical resistivity was measured under vacuum (P ~ 10 Torr) during heating and cooling with a heating rate of 1K/min. The resolution of the PPMS is in the order of 4 μΩ for a maximum applied current of 5 mA. This system allows the measurement of a sample with a maximum resistance in the order of R = 4 MΩ and a precision of 1 %.

4. Results

1. Understanding structure-property relations of perovskyte-type $LnCo_{1-x}B_xO_3$ (B = Ni, Ti) phases:

$LaCoO_3$ show potential thermoelectric properties due to its high thermopower (S ~ + 600 μV/K), but its electrical resistivity is too high (ρ ~ 10 Ω*cm). Cobalt site and lanthanum site substitution are successfully applied to tune the properties of perovskite-type cobaltate. The different substitutions in the cobal-

tates considerably improve its transport properties by changing the average oxidation state of cobalt [1, 13, 14]. *p*- and *n*-type cobaltates can be created by suitable substitutions, e.g. a low content of Ti^{4+} changes the sign of the Seebeck coefficient to negative. It is possible to improve the Seebeck coefficient values for a low substitution level and to tune the sign of the Seebeck coefficient by suitable substitutions [2, 15].

Fine powders with the composition $LaCo_{1-x}M_xO_3$ (with M = Ni, Ti and $0 \leq x \leq 0.50$) and $LnCo_{0.95}Ni_{0.05}O_3$ (Ln = La, Pr, Nd, Sm, Gd and Dy) were obtained by thermal decomposition of the corresponding amorphous citrate precursors. The diffraction patterns reveal that the $LaCo_{1-x}Ni_xO_3$ (with $0.02 < x < 0.30$) samples do not show secondary impurity phases. The Bragg reflections can be indexed in the rhombohedral structure type with $R\bar{3}c$ S.G.

Electron diffraction studies performed at room temperature reveal that $LaCo_{1-x}Ti_xO_{3-\delta}$ (with $0.10 \leq x \leq 0.50$) crystallizes in the rhombohedral structure type with $R\bar{3}c$ S.G. when $x < 0.30$, similar to the parent $LaCoO_3$ phase [16-19] and the reported $LaCo_{1-x}Ni_xO_3$ system. The powder with $x \geq 0.30$ crystallizes in the orthorhombic structure type with *Pnma (Pbnm)* S.G. similar to the $LaTiO_3$ phase [20].

The thermopower measurements of the polycrystalline $LaCo_{1-x}Ni_xO_3$ samples ($0.0 \leq x \leq 0.30$) [21], in the temperature range of $300\ K \leq T \leq 1240\ K$ and also at $T \leq 300\ K$ for x = 0.02, are presented in Figure 5. The Seebeck coefficient is positive indicating predominant positive mobile charge carriers for all the Ni-substituted compositions. The substitution of Co by Ni in the $LaCo_{1-x}Ni_xO_3$ system increases the carrier concentration, as shown in the resistivity data, leading to a reduction of the absolute Seebeck coefficient value at room temperature. In the temperature range of $250\ K < T < 300\ K$, the *S* varies only weakly with temperature. In the low substitution range where the conduction is generated by a hopping mechanism, the temperature-independent thermoelectric power can be described by Heikes formula (Eq. 1) [22]:

$$S = +\frac{k_B}{|e|} ln\left(\frac{1-c_h}{c_h}\right) \qquad \textbf{(Eq. 1)}$$

where k_B is the Boltzmann's constant and c_h is the fraction of Co site occupied by a positive charge carrier. Applying this formula to e.g. x = 0.02, the theoretical Seebeck coefficient reaches a value of S ~ + 350 µV/K, which is in good agreement with the experimental value of $S_{exp(300K)}$ = + 360 µV/K. For x = 0.10, the theoretical Seebeck coefficient adopts a value of S ~ + 200 µV/K which corresponds to $S_{exp(300K)}$ = + 173 µV/K at room temperature. In the inset of Figure 5, the room temperature values of *S* for $LaCo_{1-x}Ni_xO_3$ (scatters) are plotted as a function of nickel content x and the solid line describes the theoretical values derived from Heikes equation. The experimental room temperature data for the low substitution range, $x \leq 0.15$, are well described by Heikes formalism. However, the $LaCo_{1-x}Ni_xO_3$ becomes metallic for a higher Ni content and thus, the experimental Seebeck coefficient does not follow this theoretical approach.

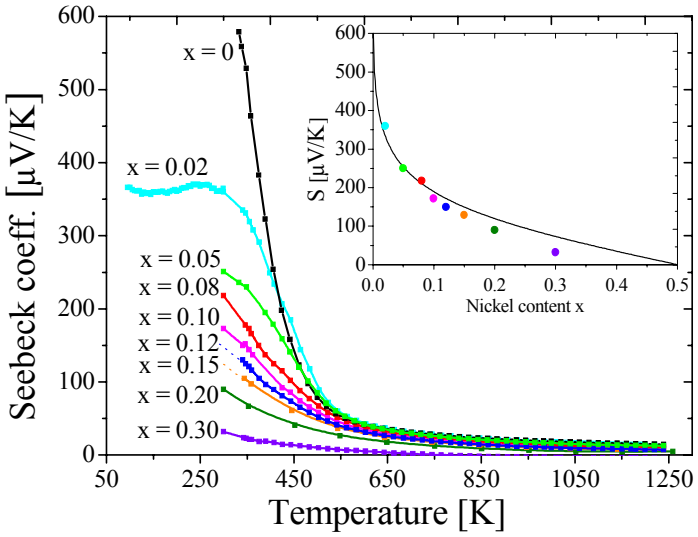

Figure 5: Thermopower of $LaCo_{1-x}Ni_xO_3$ ($0.0 \leq x \leq 0.30$) as a function of temperature in the temperature range of 300 K ≤ T ≤ 1240 K and also at T ≤ 300 K for x = 0.02; room temperature *S* data (scatters) and Heikes equation fit (solid line).

The thermoelectric Figure of merit *ZT* of the $LaCo_{1-x}Ti_xO_3$ phases (with x = 0.20, 0.30 and 0.50) is shown in Figure 6. The compounds with the highest Ti content (x = 0.50) exhibit negligible *ZT* throughout the whole temperature range, while the compounds with x = 0.20 and x= 0.30 display increasing *ZT* values with increasing temperature. The highest *ZT* with a value of ZT ~ 0.027 belongs to the $LaCo_{0.70}Ti_{0.30}O_3$ sample at T = 1120 K.

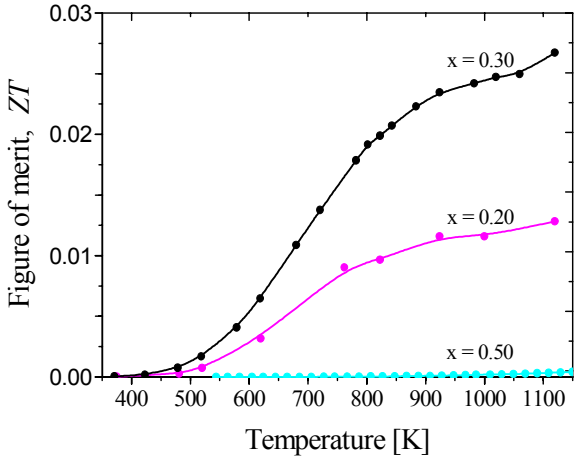

Figure 6: Thermoelectric Figure of merit *ZT* of the $LaCo_{1-x}Ti_xO_3$ compounds (with x = 0.20, 0.30 and 0.50) in the temperature range of 340 K ≤ T ≤ 1140 K.

Further investigations on the 3D cobaltates consist on the variation of the Ln element in $LaCo_{0.95}Ni_{0.05}O_3$. The principal interest of this study is related to the size of the Ln^{3+} ion. The lattice distortion introduced in the crystal structure with smaller Ln^{3+} ions has a direct impact on the stabilization of the low-spin state configuration of the Co ions, hence on the response of the thermopower with temperature. The substitution of the lanthanide element in the $LnCoO_3$ system induces structural

changes. These modifications of the unit cell parameters and the lattice distortion influence the electric transport, i.e. the Seebeck coefficient *S* and the electrical resistivity *ρ*. The temperature of the semiconductor to metal transition is increased by decreasing the rare-earth ionic radii [23]. Previous studies in the $LnCoO_3$ phases reveal a significant increase of the Seebeck coefficient at room temperature when the La cation was substituted by other rare-earth elements [24]. At the same time, an increase of the electrical resistivity was observed [23].

Our studies on the effect of Ni substitution in $LaCoO_3$ have demonstrated that large Seebeck coefficient values are kept for a low substitution level, e.g. $S_{exp(300K)}$ = + 360 µV/K for x = 0.02, while an important decrease of the electrical resistivity is observed, $\rho_{exp(300K)}$ = 70 mΩ*cm. For a higher Ni content, e.g. x = 0.10, the electrical resistivity is dramatically decreased to a value of $\rho_{exp(300K)}$ = 11.0 mΩ*cm, but also the Seebeck coefficient is lowered to a value of $S_{exp(300K)}$ = + 173 µV/K. These experimental results leads to chose x = 0.05 as the appropriate substitution level for further studies.

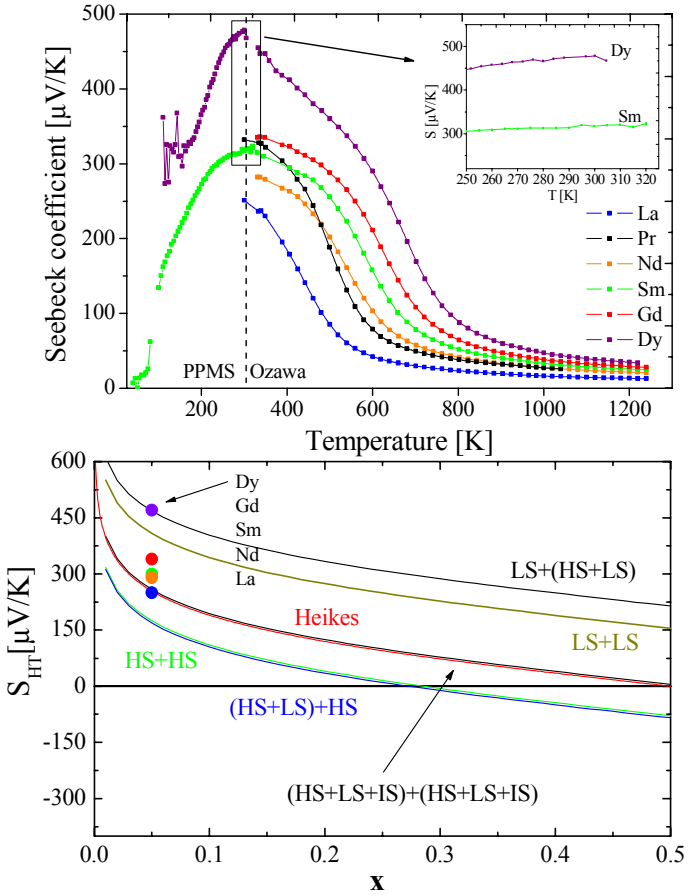

Figure 7: (above) Seebeck coefficient measurements of $LnCo_{0.95}Ni_{0.05}O_{3\pm\delta}$ (with Ln = La, Pr, Nd, Sm, Gd, and Dy) in the temperature range of 300 K < T < 1240 K, and at T ≤ 300 K for Ln = Sm and Dy); and (below) The variation of *S* calculated from the modified Heikes formula [27] with different g_3/g_4 values as a function of the charge carrier concentration x (c_h), LS, IS and HS are for low spin, intermediate spin and high spin respectively.

Figure 7 shows the Seebeck coefficient of $LnCo_{0.95}Ni_{0.05}O_{3\pm\delta}$ (with Ln = La, Pr, Nd, Sm, Gd, and Dy) in the temperature range of 330 K ≤ T ≤ 1240 K, and also at T ≤ 300 K for Ln = Dy and Sm. For all these

compounds, the Seebeck coefficient is positive indicating predominant positive charge carriers. At T = 330 K, the substitution of Co by Ni in $LnCoO_3$ increases the charge carrier concentration leading to a reduction of the absolute Seebeck coefficient value at room temperature [2]. For the $LaCoO_3$ system with a nickel content of x = 0.05, the electrical conduction is generated by a hopping mechanism and the Seebeck coefficient is weakly temperature dependent at T ≤ 300 K. The absolute Seebeck coefficient at room temperature can be estimated using the Heikes formula, valid in the high temperature limit (see Eq. 1). The Seebeck coefficient value derived from Heikes equation corresponds to $S_{Heikes,\ (x = 0.05)}$ = + 253.7 µV/K, which is very close to the experimental value of $S_{exp,\ (x = 0.05)}$ = + 251 µV/K for the La-compound at T = 300 K.

Taking into account the spin and orbital degeneracy term in the Heikes equation, the modified expression $S = +\frac{k_B}{|e|} ln\left(\frac{g_4}{g_3}\frac{1-c_h}{c_h}\right)$ **(Eq. 2)**

is obtained by Koshibae et *al.* [27], where c_h denotes the content of Co^{4+} ions and g_3 (g_4) is the number of possible configurations of the Co^{3+} (Co^{4+}) ions, which is given by the product of orbital and spin degeneracy. The $LnCoO_3$ family exhibits a different balance of spin-states of Co-III ions at room temperature [26]. Thus, the experimental *S* values for Nd- and Sm -phases are close to the theoretical fit which considers a mixture of (HS + LS + IS) for both Co^{3+} and Co^{4+} ions, while Gd-compound exhibits a experimental thermopower value closer to the theoretical fit which considers the Co^{3+} and Co^{4+} ions in the LS configurations. The Dy-compound is best described by assuming low-spin state for Co^{3+} ion and (HS + LS) for Co^{4+} ion.

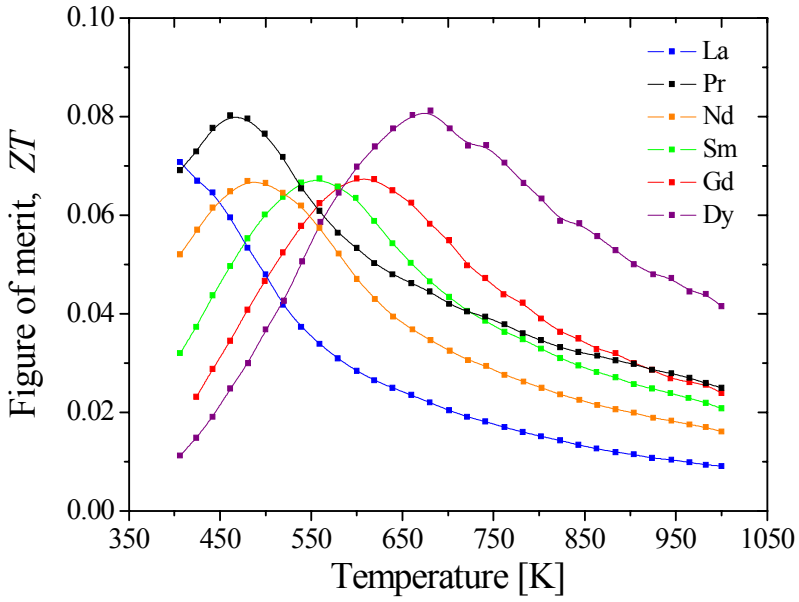

Figure 8: Thermoelectric Figure of merit *ZT* of $LnCo_{0.95}Ni_{0.05}O_{3\pm\delta}$ in the temperature range of 400 K ≤ T ≤ 1000 K.

The dimensionless Figure of merit *ZT* of the $LnCo_{0.95}Ni_{0.05}O_{3\pm\delta}$ phases adopts values in the range of ZT = $1*10^{-2}$ to ZT = $8*10^{-2}$ (see Figure 8). The best *ZT* value is observed for $LaCo_{0.95}Ni_{0.05}O_{3\pm\delta}$ with a ZT = 0.07 at T ~350 K, which is higher than the reported values of ZT = 0.022 for $LaCo_{0.80}Ni_{0.20}O_3$ [28].

2. PLD $La(CoNi)O_3$ thin films

Recently, a number of low dimension structures such as nano-structured materials, thin films, and superlattices have been proposed to improve the thermoelectric properties of materials. In particular, thin films should exhibit a decrease of the thermal conductivity due to an increased phonon scattering, while an increased local electron density of states may improve the thermopower {Hicks, 1997 #166}. Intensive research is focused on the evaluation of the thermoelectric properties of complex oxide thin films [29-32]. Epitaxial thin films grown on chemically inert single crystalline substrate materials offer a suitable alternative to large single crystals as “two-dimensional” crystal and the possibility to study the influence of the dimensionality on the thermoelectric properties.

Therefore we had studied $La(CoNi)O_3$ thin films grown on MgO (100) substrates by the Pulsed Reactive Crossed-beam Laser Ablation (PRCLA) technique. The crystallinity, morphology, composition and microstructure of the thin films are characterized. The electrical transport and thermopower of epitaxial $La(Co,Ni)O_3$ thin films have been measured in a broad temperature range and their thermoelectric activity has been compared to bulk samples. The measured films show positive Seebeck coefficient values indicative of *p*-type conduction. The thin films display a better thermoelectric performance at high temperatures compared to the polycrystalline samples.

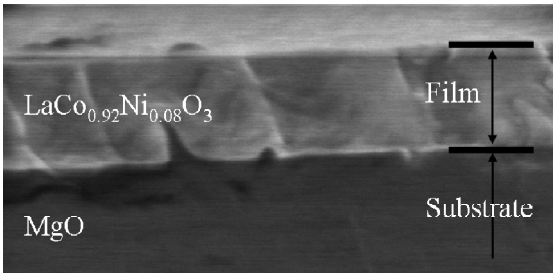

Figure 9: cross-sectional SEM-view of thin film grown on MgO.

Figure 9 shows the cross section SEM image of the thin film. The film with light contrast corresponds to the $LaCo_{0.92}Ni_{0.08}O_3$ thin film and the substrate with dark contrast corresponds to the MgO (100). The film thickness measured by a profilometer is around 86 nm with a roughness in the range of 6.9 nm and 8.1 nm. The film thickness obtain from RBS data has a value of 108 nm.

The polycrystalline cobaltate phases with a composition of $LaCo_{1-x}Ni_xO_3$ (with x = 0.05, 0.08, 0.10) crystallize in the rhombohedral structure type with $R\bar{3}c$ S.G. The thin $LaCo_{0.92}Ni_{0.08}O_3$ film has successfully been deposited on MgO substrate by PRCLA keeping the target composition. The LCNO-I thin film is highly crystalline and grows preferentially along the (100) direction of the MgO. The thermopower values upon nickel substitution in these phases are well described by Heikes equation. In thin films with low thickness, the electrical transport may be affected by the strain originating from film-substrate interface.

Above a temperature of T ~ 700 K, the Seebeck coefficient of the thin film exhibits a higher value compared to the Seebeck coefficient of the polycrystalline sample. The single crystalline $LaCo_{0.92}Ni_{0.08}O_3$ thin film exhibits a higher value of the electrical resistivity and similar value of the thermoelectric power compared with the polycrystalline sample. On the contrary, the electrical transport may be affected by the strain in the film-substrate interface. The thin film displays better thermoelectric performance at high temperatures.

3. Layered cobaltite phases: "$Ca_3Co_4O_9$"

The misfit cobaltite phases with the composition $Ca_{3-x}Ba_xCo_4O_9$ ($0.0 \leq x \leq 0.02$) and $Ca_3Co_{3.80}B_{0.20}O_9$ (with B = Fe and Ti) were obtained by thermal decomposition of the corresponding amorphous citrate precursor [1].

The crystal structure of the misfit cobaltite has an important effect on the transport properties observed in this system. The Co ions in the $[CoO_2]$ layers show a trigonal symmetry. Consequently, the electronic states of the Co ions in an octahedral field, i.e. t_{2g} and e_g orbitals, further degenerate into the non-degenerated a_{1g} and the twofold degenerated e_g' orbitals. Large density of states at the Fermi level (E_F) found in the narrow a_{1g} band are responsible for the large Seebeck coefficient, while charge carriers in the e_g' band are responsible for the metallic conductivity [14].

The layered structure of the misfit cobaltite consists of the stacking of the layers with a common *c* lattice parameter (*c* = 10.6 Å):

i) A triple $[AO]_\infty$ layer with *A* = Ca, Co leading to the rock-salt type layer.

ii) A $[CoO_2]$ hexagonal layer generating the subsystem which displays a distorted CdI_2-type structure with lattice parameters $a \approx b_2\sqrt{3}$ stacked along [001] [33, 34]. The $[CoO_2]$ layers can be distinguished in the HREM image as the darker lines.

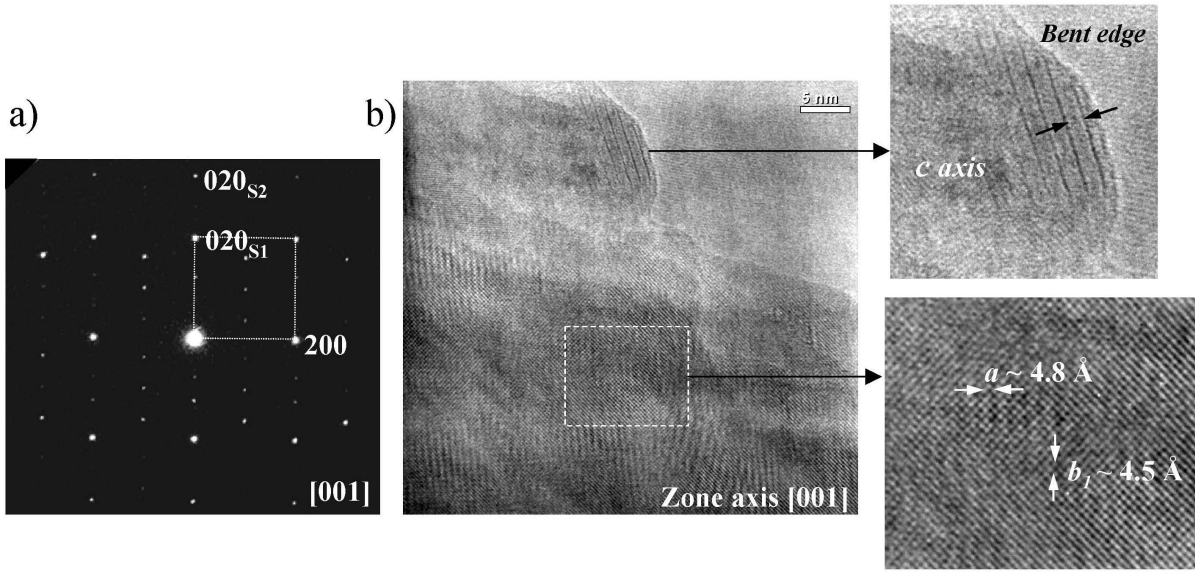

Figure 10: a) Electron diffraction (ED) pattern and b) HREM image on the zone axis [001].

The Seebeck coefficient values for all the misfit cobaltites are positive indicating *p*-type conduction. The thermopower of the misfit phase is relatively large (S = + 120 µV/K) at room temperature despite of the metallic behaviour.

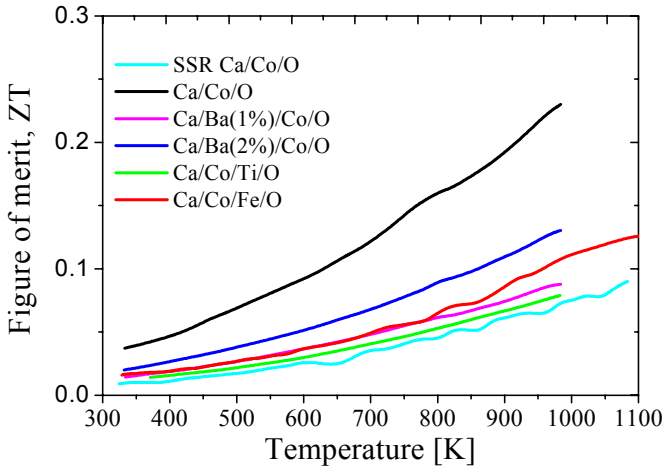

Figure 11: Figure of merit for the misfit phases in the temperature range of 340 K ≤ T ≤ 1100K.

Figure 11 shows the temperature dependence of the Figure of merit, in the temperature range of 340 K ≤ T ≤ 1100 K. For all the samples, the *ZT* increases with increasing temperature. The misfit cobaltite compound prepared by soft chemistry route exhibits the highest *ZT* values over the measured temperature range and reaches a value of ZT = 0.23 at T = 985 K, which is in good agreement with reported *ZT* values of polycrystalline sample at high temperature, e.g ZT ~ 0.22 at T = 1000 K for spark plasma sintered $Ca_3Co_4O_9$ [35].

5. Discussion

This work is dedicated to the study of high temperature thermoelectric properties of perovskite-type and layered complex cobalt oxide phases. The enhancement of the thermoelectric Figure of merit of a material, defined as $ZT = S^2T/\rho\kappa$; remains a challenge to be solved considering that S, ρ and κ are interdependent.

Among the oxides, lanthanum cobalt oxide perovskites are good starting materials for developing potential thermoelements owing to the fact that they exhibit semiconducting electrical conductivity and a large Seebeck coefficient at room temperature. Layered cobaltites also posses a large thermopower together with a metallic electrical conductivity and a low thermal conductivity typical for a “phonon glass electron crystal”. Additionally, cobaltite phases display enhanced thermoelectric properties at high temperatures.

The polycrystalline cobaltate phases with various compositions and mesoporous morphology are successfully synthesised by a soft chemistry method based on the chelation of metals with citric acid in aqueous solution. The products are characterized concerning phase crystallinity, thermal stability, composition and microstructure. The heat and electric transport in these phases is evaluated in a wide temperature range. The Figure of merit *ZT* of the materials is determined. Summarising, this work

relates morphology, composition and crystal structure of these phases to the measured transport properties.

In this experimental study the influence of *A*- and *B*- site substitution in the $LaCoO_3$ system is reported. The Co-substituted phases crystallize in rhombohedral symmetry with $R\bar{3}c$ S. G. Thermogravimetric studies confirm the thermal stability of these phases up to T = 1273 K. The effect of partial substitution of the Co-site by Ni considerably improves the transport properties by changing the valence state of Co. EXAFS data evaluation revealed a reduction of the Co-O bond length in the CoO_6 octhaedra upon increasing Ni content. From these results it can be concluded that Ni substitution leads to the formation of smaller Co^{+4} ions. The decrease of the electrical resistivity, observed when the Ni content increases, can be attributed to the increase of Co^{4+} ions and thus, to the number of holes in the mixed ($Co^{3+/4+}$) valence band. The temperature dependence of the electrical resistivity follows ($\rho(T) \sim exp(E_a/kT)$), as expected for a thermally activated process. The activation energy E_a decreases with increasing Ni content. The electrical resistivity values of polycrystalline pressed pellets are similar to the reported values for single crystals. These results lead to the conclusion that the grain boundaries and pores do not hinder the electrical transport. The thermopower of these phases is positive indicating that the electronic transport is made by holes-like carriers. Large *S* is preserved for low level substitution in good accordance with the Heikes equation $S = +\frac{k_B}{|e|} ln\left(\frac{1-c_h}{c_h}\right)$. The Seebeck coefficient of non- and slightly substituted $LaCoO_3$ phases is high and weakly temperature dependent (S ~ 1/T) in the temperature region of 150 K < T < 310 K. The results indicate that holes are more mobile. In the $LaCoO_3$, *B*- site substitution by Ni reveals that the charge carrier concentration plays an important role in the enhancement of the power factor. The highest power factor value belongs to the 5 % Ni-substituted compound.

The sign of the Seebeck coefficient can be changed by suitable substitutions. 1 % Ti content on the $LaCoO_3$ leads to a sign change of *S* to a negative value. The thermopower has a value of S = - 216 µV/K at T = 330 K. A negative Seebeck coefficient indicates that the predominant charge carriers in the $LaCo_{0.99}Ti_{0.01}O_3$ are electrons. Electron carriers are induced by substitution of Co^{3+} ions by Ti^{4+} ions with the subsequent creation of Co^{2+} ions. This assumption is confirmed by XANES experiments. The electrical resistivity of this phase is high. This observation is explained by the fact that the hopping in the e_g band of the 3*d* orbital in the mixed Co^{2+}/Co^{3+} valence is not possible by moving only one electron. As a result, ρ is lowered by a spin-blockade. The $LaCo_{1-x}Ti_xO_3$ (with x < 0.30) crystallises in rhombohedral symmetry as the Ni substituted phases. For a higher Ti content (x ≥ 0.30), the structure changes to orthorhombic symmetry. The thermopower of the orthorhombic phases is large and positive e.g. $S_{(x = 0.30,\ T = 350K)}$ = + 520 µV/K. The *S* values evidence a hole-doped electrical conduction mechanism which is compatible with an activated regime for the hopping of charge carriers in a matrix of high spin Co^{2+}. These results indicate that the relative amount of high-spin, intermediate-spin and low-spin trivalent cobalt ions in $LaCo_{1-x}Ti_xO_{3-\delta}$ may change with the Ti^{4+} content. The lattice thermal conductivity of the $LaCo_{1-x}Ti_xO_3$ phases is low and nearly constant with temperature. κ_{ph} values are in the range of 0.4 W/m*K < κ_{ph} < 1.0 W/m*K. These results can be attributed to an increase of the lattice disorder induced by the atomic disarray on the *B*-site of the perovskite. The polycrystalline samples exhibit very small crystallite sizes in the range of few nanometers. Therefore, another possible phonon

scattering process which may take place is the phonon scattering by grain boundaries. The Figure of merit of these materials increases with increasing temperature. These results evidence the potential of the La(Co,Ti)O_3 phases for applications as high temperature thermoelectric materials.

The $LnCo_{0.95}Ni_{0.05}O_3$ (with Ln = Pr, Nd, Sm, and Gd) phases crystallize in the orthorhombic lattice with *Pbnm* S.G with exception of the La-phase which crystallizes in the monoclinic structure type with *I*2/*a* S.G. Electron diffraction studies show that the crystal symmetry of the La-compound is better described with a monoclinic *I*2/*a* S.G. rather than with the rhombohedral $R\bar{3}c$ S.G. In these phases, the modifications of the unit cell parameters and the lattice distortion influence the electric transport. The results show that the decrease of the Ln ionic radii results in a decrease of the M-O-M bond angle. Consequently, the ρ increases systematically as a result of the decrease in the overlapping of the oxygen 2*p* and the metal 3*d* orbitals. The value of the Seebeck coefficient increases at room temperature when the size of the rare-earth element is decreased. The thermopower observed in $LaCo_{0.95}Ni_{0.05}O_3$ (S_{exp} = + 253.7 µV/K) agrees with the theoretical Heikes value of S_{Heikes} = + 251 µV/K calculated for a concentration of charge carriers of c_h = 0.05. However, the thermopower of the Dy-compound is best described by the generalized Heikes formula ($S = S_{Heikes} + S_{spin+orbit}$) which takes also into account the spin and orbital degeneracy of the Co ions. This term, calculated for the low-spin states of Co^{3+} (t_{2g}^6) and Co^{4+}(t_{2g}^5), gives a value of $S_{spin+orbit} = +\frac{k_B}{|e|} ln\left(\frac{1}{6}\right)$ = + 154 µV/K. Thus, the thermopower considering S_{Heikes} and $S_{spin+orbit}$ results in a value of S = + 405 µV/K, which gives a better agreement with the experimental value of S = + 450 µV/K displayed by the Dy-compound. From the observed Seebeck coefficient results it can be concluded that the $LnCoO_3$ family exhibit different balance of spin states of Co-III ions at room temperature. Furthermore, small Ln ions stabilise the low-spin state configuration of the Co ions. Heat transport measurements reveal that in these phases the heat is carried predominantly by phonons. The best *ZT* value (ZT = 0.07) is observed for the $LaCo_{0.95}Ni_{0.05}O_{3\pm\delta}$ compound at T ~ 350 K. The Dy-compound has a value of ZT = 0.081 at T = 660 K which is the highest reported value for these compounds at high temperature.

The single crystalline $LaCo_{0.92}Ni_{0.08}O_3$ thin film exhibits a higher value of the electrical resistivity and similar value of the thermoelectric power compared with the polycrystalline sample. These results show that the Seebeck coefficient is not sensitive to the sample dimensions. On the contrary, the electrical transport may be affected by the strain in the film-substrate interface. The thin films display better thermoelectric performance at high temperatures.

The thermoelectric properties of $Ca_3Co_4O_9$ and substituted cobaltite phases are evaluated. $Ca_3Co_4O_9$ has been synthesized by solid state reaction (SSR) and “chimie douce” methods. The results show that the heat and electrical transport in the layered cobaltite is influenced by the synthesis procedure. The compound synthesized by solid state reaction exhibits resistivity values comparable to reported literature data. However, the resistivity is three times higher than the compound prepared by “chimie douce”. The reason for the higher resistivity value found in the SSR-cobaltite can be attributed to small amount of oxide impurities. Thus, samples prepared by SSR method leads to a less chemically homogeneous composition as a result of diffusion processes. In the substituted phases, the observed different electrical resistivity values may be ascribed to changes of the oxygen content and of the Co

oxidation valence state in the rock-salt layer. However, it should be pointed out that substitution effects are hard to predict since the Co valence state distribution in the compound is not clear yet. Heat transport measurements reveal that the major contribution to the thermal conductivity comes from the lattice component. The thermal conductivity is governed by the crystallographic structure of the cobaltite and the κ_l is suppressed by phonon scattering at the interface of the two types of Co-O layers. The experimental thermogravimetry data show that the oxygen content in the misfit compound changes with temperature. An increase in temperature leads to thermal reduction while a decrease leads to re-oxidization. The Seebeck coefficient values for all the misfit phases are positive indicating *p*-type conduction. All misfit compounds present a similar Seebeck coefficient value in the range of + 119 μV/K ≤ S ≤ 121.3 μV/K at T = 330 K, independently from substitution. These thermopower values are large in spite of the metallic-like behaviour of the electrical resistivity at room temperature. The experimental thermoelectric power is fitted using the generalized Heikes equation, assuming that the both Co^{3+} and Co^{4+} ions are in the low-spin state and a Co valency of $\upsilon_{Co} \approx 3.6$ in the CoO_6 layer. From the present Seebeck coefficient results at room temperature it can be concluded that the different substitutions in the cobaltite system take place in the rock-salt subsystem. Furthermore, the spin-orbit degeneracy term gives the main contribution to the thermopower. The thermoelectric properties displayed by the misfit cobaltites i.e. a large Seebeck coefficient, poor thermal conduction together with a metal-like good electrical conduction demonstrate the large potential of these oxides for high temperature applications.

6. Conclusions

The present study illustrates the challenge in obtaining materials with good thermoelectric properties. It has been shown that a low substitution level results in large Seebeck coefficient and lower electrical resistivity values. Additionally, high thermopower results when the Co ions are in the low-spin state configuration. Thus, *S* values are tuned by varying the charge carrier concentration and/or the spin degeneracy term. Additionally, materials with small particles size morphology and complex structures have shown to reduce the lattice thermal conductivity.

A proposed future work related to the present study will be to perform in-situ high temperature measurements. These experiments can yield information about structure on different length scales, phase and chemical composition, dynamic phase formation, phase decomposition and phase transition processes which can influence the materials behaviour at the operational temperature in the application.

Referenzen

[1.] Robert R., Romer S., Reller A., and Weidenkaff A., Adv. Eng. Mater., 7 (2005) 303-308.
[2.] Robert R., Bocher L., Trottmann M., Reller A., and Weidenkaff A., J. Solid State Chem., 179 (2006) 3867–3873.
[3.] Robert R. and Weidenkaff A., BfE-Abschlussbericht, (2006)
[4.] Terasaki I., Sasago Y., and Uchinokura K., Phys. Rev. B, 56 (1997) R12 685-R12 687.
[5.] Takada K., Nature, 422 (2003) 53-55.
[6.] Pechini M. P., *Patent*. 1967: US
[7.] Krupicka E., Reller A., and Weidenkaff A., Crys. Eng., 5 (2002) 195-202.
[8.] Weidenkaff A., Adv. Eng. Mater., 6 (2004) 709-714.
[9.] Bocher L., Aguirre M. H., Robert R., Trottmann M., Logvinovich D., Hug P., and Weidenkaff A., Thermochim. Acta, doi: 10.1016/j.tca.2007.02.013. (2007)
[10.] Montenegro M. J., Döbeli M., Lippert T., Müller S., Schnyder B., Weidenkaff A., Willmott P. R., and Wokaun A., Phys. Chem. Chem. Phys., 4 (2002) 2799-2805.
[11.] Montenegro M. J., Lippert T., Müller S., Weidenkaff A., Willmott P. R., and Wokaun A., Appl. Surf. Sci., 197 (2002) 505-511.
[12.] Montenegro M. J., Clerc C., Lippert T., Müller S., Willmott P. R., Weidenkaff A., and Wokaun A., Appl. Surf. Sci., 208 (2003) 45-51.
[13.] Maignan A., Hébert S., Pi L., D. Pelloquin, Martin C., Michel C., M. Hervieu, and Raveau B., Cryst. Eng., 5 (2002) 365–382.
[14.] Miyazaki Y., Solid State Ionics, 172 (2004) 463-467.
[15.] Hébert S., Flahaut D., Martin C., Lemonnier S., Noudem J., Goupil C., and Maignan A., Prog. Solid State Chem., 35 (2007) 457-467.
[16.] Raccah P. M. and Goodenough J. B., Phys. Rev. B, 155 (1967) 932-943.
[17.] Thornton G., Tofield B. C., and Williams D. E., Solid State Commun., 44 (1982) 1213-1216.
[18.] Thornton G., Tofield B. C., and Hewat A. W., J. Solid State Chem., 61 (1986) 301-307.
[19.] Radaelli P. G. and Cheong S.-W., Phys. Rev. B, 66 (2002) 094408.
[20.] Sunstrom-IV J. and Kauzlarich S., Chem. Mater., 5 (1993) 1539.
[21.] Robert R., Bocher L., Sipos B., Döbeli M., and Weidenkaff A., Prog. Solid State Chem., 35 (2007) 447-455.
[22.] Heikes R. R., Mazelsky R., and Miller R. C., Physica 30, 8 (1964) 1600-1608.
[23.] Yamaguchi S., Okimoto Y., and Tokura Y., Phys. Rev. B, 54 (1996) R11 022-R11 025.
[24.] Knížek K., Jirák Z., Hejtmánek J., Veverka M., Maryško M., Maris G., and Palastra T. T. M., The European Physical Journal B, 47 (2005) 213-220.
[25.] Hwang H. Y., Cheong S.-W., Radaelli P. G., Marezio M., and Batlogg B., Phys. Rev. Lett., 75 (1995)
[26.] Zhou J. S., Yan J. Q., and Goodenough J. B., Phys. Rev. B, 71 (2005) 220103-1.
[27.] Koshibae W., Tsutsui K., and Maekawa S., Phys. Rev. B, 62 (2000) 6869-6872.
[28.] Migiakis P., Androulakis J., and Giapintzakis J., J. Appl. Phys., 94 (2003) 7616-7620.
[29.] Terada T., Yoshida Y., Ueno M., and Takai Y., J. Ceram. Soc. Jpn., 110 (2002) 560-563.
[30.] Moyer J. G., Kukuruznyak D. A., Nguyen N., Prowse M. S., and Ohuchi F. S., J. Appl. Phys. , 100 (2006) 083504 -083517.
[31.] Eng H. W., Prellier W., Hébert S., Grebille D., Mechin L., and Mercey B., J. App. Phys., 97 (2005) 013706.
[32.] Sakai A., Kanno T., Yotsuhashi S., Okada S., and Adachi H., J. App. Phys., 99 (2006) 093704.
[33.] Masset A. C., Michel C., A. Maignan, Hervieu M., O.Toulemonde, Studer F., B. Raveau, and Hejtmanek J., Phys. Rev. B, 62 (2000) 166.
[34.] Lambert S., Leligny H., and Grebille D., J. Solid State Chem., 160 (2001) 322-331.
[35.] Wang D., Chen L., Yao Q., and Li J., Solid State Commun., 129 (2004) 615-618.